

## PHYSICS

# Postselection shifts the transition frequency of helium in an atomic beam

Jin-Lu Wen<sup>1†</sup>, Jia-Dong Tang<sup>2†</sup>, Ya-Nan Lv<sup>2†</sup>, Yu R. Sun<sup>3\*</sup>, Chang-Ling Zou<sup>4,5\*</sup>, Jun-Feng Dong<sup>5</sup>, Shui-Ming Hu<sup>1,2,5\*</sup>

Postselecting output states can effectively amplify weak signals in measurements. However, the postselection (PS) effect may also introduce unintended biases in precision measurements. Here, we investigate the influence of PS in the precision spectroscopy of the  $2^3S - 2^3P$  transition of helium ( $^4\text{He}$ ) using an atomic beam. We directly observe that PS based on atomic positions causes a shift in the measured transition frequency, amounting to approximately  $-55$  kHz. After accounting for this PS shift, we obtain a corrected frequency of  $276,764,094,712.45 \pm 0.86$  kHz for the  $2^3S_1 - 2^3P_0$  transition. Combining this result with existing data for  $^3\text{He}$ , we derive a value for the difference in squared nuclear charge radii, which shows a  $2.6\sigma$  deviation from measurements of muonic helium ions, potentially pointing to new physics that challenges lepton universality in quantum electrodynamics.

## INTRODUCTION

Over the past few decades, quantum mechanics has profoundly reshaped our understanding of nature, facilitating the development of technologies that defy classical intuitions. One of the intriguing quantum effects is postselection (PS) and weak value amplification (WVA) (1–3). By selectively detecting outcomes in a weak interaction measurement, PS and WVA can enhance the measurement signal, though this comes at the cost of discarding part of the observed data (4). Despite some controversy surrounding its counterintuitive nature in recent years (5), WVA has found applications in precision measurement (6) and inspired ideas in quantum technologies (7–13). This quantum mechanical effect has particular relevance for precision measurements, where even very tiny spectroscopic shifts in atoms and molecules can be crucial for tasks such as maintaining accurate time (14), detecting weak forces (15, 16), and testing fundamental physical models (17, 18). Although PS can enhance the precision of measurements involving multiple degrees of freedom, it may also introduce systematic shifts that must be carefully accounted for.

In this work, we investigate the impact of PS on the precision spectroscopy of the  $2^3S - 2^3P$  transition of  $^4\text{He}$  in an atomic beam. We observed an unexpected discrepancy in the results depending on how the experimental data are analyzed, which we attribute to PS effects. This interpretation is supported by theoretical analysis and simulations. Our findings underscore the importance of carefully considering subtle quantum effects, like PS, in high-precision measurements.

Precise measurements of helium atom transition frequencies have long been used to determine nuclear charge radii, as electron penetration into the non-point-like nucleus causes energy level shifts that depend on the nucleus's size. Recent spectroscopy (19–21) of the

$2^3S - 2^1S$  transitions in  $^3\text{He}$  and  $^4\text{He}$  provided the difference between the squared charge radii of these two nuclei,  $\delta r^2 [r_h^2 - r_\alpha^2] = r^2(^3\text{He}) - r^2(^4\text{He})$ . This result deviated by  $3.6\sigma$  from measurements derived from spectroscopy (22, 23) of the muonic helium ion ( $\mu\text{-He}^+$ ), in which the electron is replaced by a muon. A similar discrepancy was noted in measurements of the proton charge radius, which has been studied extensively using hydrogen atom ( $e\text{-H}$ ) spectroscopy (24), but shows a notable deviation when measured using muonic hydrogen ( $\mu\text{-H}$ ) (25), leading to the well-known “proton radius puzzle.” In light of these findings, our results of  $^4\text{He}$ , combined with the  $^3\text{He}$  result of Cancio Pastor *et al.* (26), allow us to compare the  $\delta r^2$  value from  $e\text{-He}$  spectroscopy with that from the precise spectroscopy of  $\mu\text{-He}^+$ , providing a test of the equivalence of leptons in lepton-nucleus interactions (27). Should these deviations be confirmed, they could pose a substantial challenge to the Standard Model, as the muon and electron are believed to share identical electromagnetic properties in quantum electrodynamics.

## RESULTS

### Experimental observation of the PS effect

We used an atomic beam to measure the  $2^3S - 2^3P$  transition of helium and determine the nuclear charge radii difference between  $^3\text{He}$  and  $^4\text{He}$  (20, 21, 26, 28–30). Figure 1 shows the experimental setup, where a collimated beam of helium atoms interacts with probe lasers. Atoms with specific internal and external states pass through a slit (slit 3 in Fig. 1) before reaching the detector. This method, first proposed by Ramsey (31), has been widely adopted in precision measurements due to its simplicity and ability to explore systematic uncertainties. In our experiment, we applied the SCTOP (sequential counterpropagating traveling-wave optical probing) method (32), which involves three key steps: (i) State preparation: Helium atoms are prepared in the  $|M_J = \pm 1\rangle$  levels of the  $2^3S_1$  metastable state, the lateral momentum of the atoms is denoted as  $p = mv_x$ , while the longitudinal velocity  $v_z$  can be adjusted within the range of 100 to 400 m/s with a spread of about  $\pm 5$  m/s (33). (ii) Interrogation: The atomic transition is probed by a tunable 1083-nm laser. When the laser is resonant with the transition to the  $2^3P_0$  state, atoms are probably to absorb photons and spontaneously decay (with a natural lifetime of 98 ns) to the  $|M_J = 0\rangle$  ground state. To eliminate the

<sup>1</sup>State Key Laboratory of Molecular Reaction Dynamics, Department of Chemical Physics, University of Science and Technology of China, Hefei 230026, China. <sup>2</sup>Hefei National Research Center of Physical Sciences at the Microscale, University of Science and Technology of China, Hefei 230026, China. <sup>3</sup>Institute of Advanced Science Facilities, Shenzhen 518107, China. <sup>4</sup>CAS Key Laboratory of Quantum Information, University of Science and Technology of China, Hefei 230026, China. <sup>5</sup>Hefei National Laboratory, University of Science and Technology of China, Hefei 230088, China.

\*Corresponding author. Email: sunyu@mail.iasf.ac.cn (Y.R.S.); clzou321@ustc.edu.cn (C.-L.Z.); smhu@ustc.edu.cn (S.-M.H.)

†These authors contributed equally to this work.

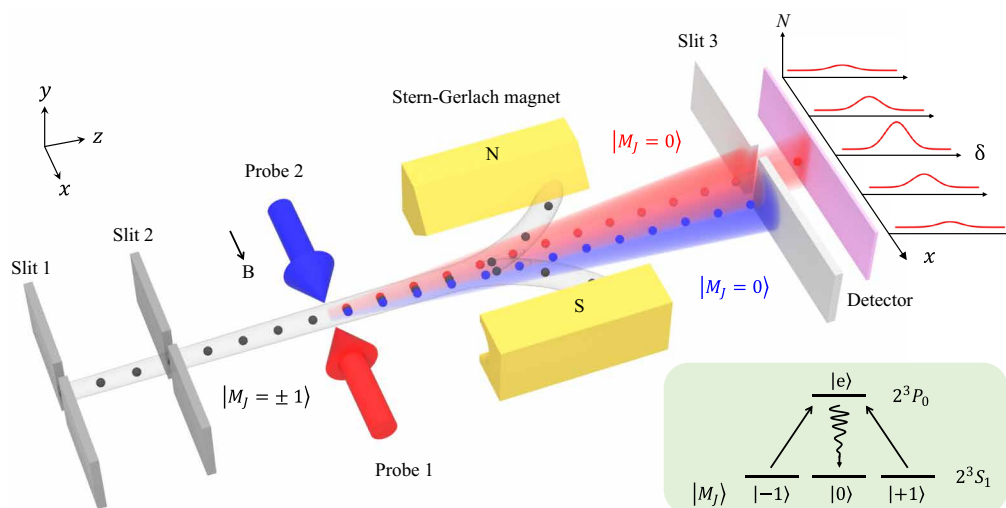


**Fig. 1. Experimental setup of precision spectroscopy of atomic helium with postselection.** A collimated helium atomic beam is prepared in the  $M_J = \pm 1$  levels of the  $2^3S_1$  state (lifetime  $\tau \sim 7900$  s). The probe laser is scanned around the resonance of the  $2^3S_1 - 2^3P_0$  transition. Two counterpropagating probe laser beams, labeled “probe 1” and “probe 2,” are periodically blocked, so that at any given time, only one beam interacts with the atoms. Atoms excited by the probe laser to the  $2^3P_0$ ,  $M_J = 0$  state undergo spontaneous decay ( $\tau \sim 98$  ns) to either the  $2^3S_1$ ,  $M_J = 0$  or  $2^3S_1$ ,  $M_J = \pm 1$  levels. Atoms in the  $M_J = \pm 1$  states are deflected by a Stern-Gerlach magnet and removed from the atomic beam, while only atoms in the  $M_J = 0$  state pass through a narrow slit (width  $\Delta x_s \sim 0.3$  mm) placed before a multichannel plate detector. These atoms, shown as blue and red spheres, correspond to atoms interacting with probe 1 and probe 2, respectively. The slit can be moved along the  $x$  axis to select atoms with specific momenta. As atoms absorb and emit photons during the interaction, their velocity in the  $x$  direction changes, affecting the position where they reach the slit. For a given  $x$  position of the slit, spectra are recorded by counting the number of detected atoms ( $N$ ) while scanning the laser frequency ( $\delta$ ). The central frequencies obtained from both probe beams are averaged to eliminate the first-order Doppler shift.

first-order Doppler shift caused by atoms with nonzero lateral velocity  $v_x$ , two counterpropagating laser beams are used (32). (iii) Detection: Only the atoms in the  $|M_J = 0\rangle$  state pass through a Stern-Gerlach magnet (SGM) without deflection and are collected by a micro-channel plate (MCP) detector for counting.

During the interrogation, changes in the internal atomic state are linked to changes in external degrees of freedom. After absorbing and emitting photons, the lateral momentum of a helium atom changes from  $p = mv_x$  to  $p = mv_x + \hbar k - \hbar r$ , where  $\hbar k$  is the momentum of the probe laser photon and  $\hbar r$  represents the randomly emitted photon. Repeated absorption and emission cycles can cause notable momentum shifts as the atom transitions between internal states ( $|M_J = \pm 1\rangle$  to  $|M_J = 0\rangle$ ), creating an entanglement between momentum change and atomic-state transitions. This entanglement allows for WVA of atomic momentum, as schematically illustrated in Fig. 1. By selecting atoms based on their position  $x$  (i.e., notably away from the center), we can observe large momentum shifts associated with considerable changes in the resonance frequency, together with a reduced number of detected atoms. Measurements of the amplified Doppler shift enable a precise evaluation of the systematic shift, facilitating the determination of the transition frequency. We placed a narrow slit in front of the detector to select atoms with specific momenta based on the location of the narrow slit ( $x$ ). In addition, the two counterpropagating probes (“probe 1” and “probe 2”) were alternatively blocked (32), and two spectra were recorded at each  $x$ . A feedback servo system was used to ensure the angle deviation between the two beam directions remains below  $1 \times 10^{-5}$  rad.

Figure 2A illustrates the relationship between the detected number of atoms and their position  $x$  and the frequency of probe 1, with an atomic velocity of  $v_z = 290$  m/s. Most detected atoms are located

near the origin  $x \approx 0$  but show a slight shift along the  $x$  direction due to the probe laser. We obtained a spectrum at each  $x$ . For instance, the spectrum indicated by solid triangles in Fig. 2B corresponds to the location  $x = 0.6$  mm marked by the dashed-dotted line in Fig. 2A. Each spectrum was fitted using a Lorentzian function, and the fitted center, along with its uncertainty, is represented as a blue triangle with an error bar in Fig. 2E. The observed line width is approximately 2.2 MHz, which aligns with the natural linewidth of the  $2^3S - 2^3P$  transition (1.6 MHz). When only the counterpropagating probe laser (probe 2) was used, results are depicted in Fig. 2 (C and D), with the fitted spectral centers shown as green triangles in Fig. 2E. Notably, signals weaken substantially at larger  $x$  positions, leading us to include only results for  $|x| < 0.7$  mm in Fig. 2E. A linear fit of the blue and green dotted lines indicates that the spectral center varies linearly with  $x$ , suggesting a Doppler shift as the probe interacts with atoms. The fitted slope is approximately 0.09 MHz/mm, consistent with the calculated Doppler shift at  $v_d = v_z(x/L)$ , where  $L$  is the distance from the probe laser to the slit. Comparing results from the two probing directions reveals that the shift averages out for each pair of centers obtained at the same slit position. This yields a result that is independent of  $x$ , as represented by the red dotted lines in Fig. 2 (E and F).

To assess the effect of PS, we contrast the results obtained with and without PS of final states. By averaging the counts over  $x$  for all data in Fig. 2 (A and C), we derive two spectra, shown as open circles in Fig. 2 (B and D). Removing the slit in front of the detector yields identical spectra. Both spectra were fitted with Lorentzian functions, with their centers illustrated as blue and green lines in Fig. 2F. The mean value of these centers is marked by the red solid line. A notable deviation of about  $-55$  kHz is observed between the results with and without PS, despite using the same experimental

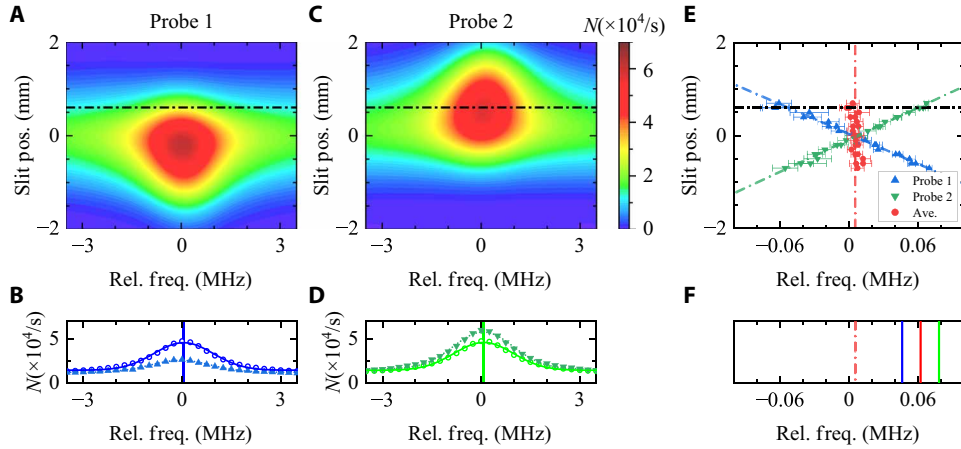


**Fig. 2. Experimental data of the spectroscopy of the  $2^3S - 2^3P$  transition in a  $^4\text{He}$  atomic beam probed by the SCTOP method.** (A) Experimental data recorded by probe 1 at different slit positions along the  $x$  axis. (B) Solid triangles represent the spectrum obtained with PS of atoms at the position  $x = +0.6$  mm [dashed-dotted line in (A)], while open circles show the spectrum without PS. (C and D) The corresponding results obtained with probe 2. (E) Center frequencies of the spectra with PS at each  $x$  position for probe 1 (blue up-triangles) and probe 2 (green down-triangles). Averaged center frequencies at various  $x$  positions are shown as red solid circles. (F) Center frequencies obtained with PS (red dotted line) compared to those without PS (solid lines). The blue and green lines correspond to center frequencies without PS for probe 1 and probe 2, respectively, and their average is represented by the red solid line.

data. Measurement conducted without the slit also yielded results consistent with this value, albeit without the PS effect.

### Theoretical interpretation

The expected number of collected atoms through slit 3 could be written as  $N(\delta) \propto |\langle \psi_f(p) | \langle 0 | U_{SE} O(\delta) | \pm 1 \rangle | \psi_i(p) \rangle|^2$ , where  $\psi_{i/f}(p)$  represents the initial/final momentum wave functions of the atom,  $O(\delta)$  describes the weak transition operator, flipping the internal state of the atom while transferring momentum between the photon and atom, with detuning  $\delta$ , and  $U_{SE}$  denotes the evolution operator for spontaneous radiation from the excited state  $|e\rangle$ . To simplify the model and avoid directly solving the operator  $O$ , we consider the velocity distributions of the atoms in the lateral ( $x$ ) direction. The resulting number of collected atoms is approximately

$$N(\delta) \propto \iint dv_0 dv_1 \frac{P_0(v_0) P_t(v_0, v_1) P_1(v_1)}{(\delta - kv_0)^2 + \gamma^2} \quad (1)$$

where  $P_0(v_0) = e^{-(v_0 - v_{0,b})^2 / 2\sigma_0^2}$  represents the velocity distributions of initial atoms with a bias velocity  $v_{0,b}$  and spread  $\sigma_0$ ;  $P_1(v_1) = e^{-(v_1 - \xi x)^2 / 2\sigma_1^2}$  is the velocity distribution of the detected atoms passing through the slit, where  $\xi x$  is the bias velocity at detection,  $\xi$  depends on the time of flight, and  $\sigma_1$  is the velocity spread at detection;  $P_t(v_0, v_1) = \frac{1}{2} \sqrt{1 - (v_1 - v_0 - v_R)^2 / v_R^2}$  for  $0 \leq \frac{1}{2} |v_1 - v_0| \leq v_R$  is the probability distribution for lateral velocity change from  $v_0$  to  $v_1$  due to absorption and spontaneous emission of photons, with  $v_R = \hbar k / m$ . Because in practice  $v_R \ll \sigma_{0,1}$ , we can approximate the number of atoms as  $N(\delta) \propto \int dv_0 \frac{P_0(v_0) P_1(v_0 + v_R)}{(\delta - kv_0)^2 + \gamma^2}$ . In the case of a narrow slit in front of the detector ( $\sigma_1 \ll \sigma_0$ ), the center of the spectrum for probe 1 can be approximated as  $\delta_{PS,+} = k(\xi x - v_R)$ , and for probe 2, the center is  $\delta_{PS,-} = -k(\xi x + v_R)$ . The PS can indeed produce a considerable Doppler shift in the measured spectral center, which is linearly dependent on the slit position  $x$ . This

observation aligns with the results presented in Fig. 2E. For measurements without PS, where the detector slit is wide enough that  $\sigma_1 \gg \gamma/k$ , the atomic velocity distribution  $P_1(v_0 + v_R)$  can be approximated as constant. In this case, the spectral centers are primarily determined by the initial distribution of the atomic velocity, yielding shifts of  $\delta_{NPS,+} \approx kv_{0,b}$  for probe 1 and  $\delta_{NPS,-} \approx -kv_{0,b}$  for probe 2. Notably, the  $v_{0,b}$ -dependent frequency shift can be mitigated by averaging the measured spectral centers obtained with counterpropagating probe lasers. However, for the PS scenario, a residual frequency shift of  $(\delta_{PS,+} + \delta_{PS,-}) / 2 = -kv_R$  persists when compared to results without PS. This shift is attributed to the recoil of the atoms upon photon absorption, as illustrated in Fig. 2F.

The experimental results can also be understood through a phenomenological model (see the Supplementary Materials), as depicted in Fig. 3. Two slits are used to select atoms with zero velocity along the axis of the probing laser beams. When an atom absorbs a photon from the probe 1 laser, its momentum changes. Only atoms with a specific negative initial velocity of  $-v_R \frac{L}{\ell + L}$  along the  $x$  direction, counterpropagating to the probe 1 beam, can pass the second slit and

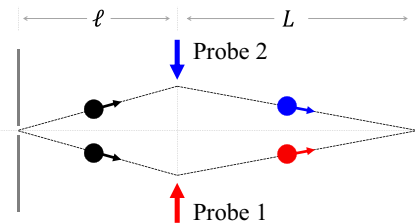


**Fig. 3. A phenomenological model of the PS effect.** Two slits were placed to select atoms with a zero velocity along the  $x$  axis. However, owing to the momentum change after absorbing a photon from the probing laser, only atoms with a non-zero initial velocity  $v_x \approx v_R \frac{L}{\ell + L}$  can pass the second slit, which induces a red shift in the center frequency. Note that the same shift applies with a counterpropagating probe beam (probe 2).

be detected, where  $v_R$  is the recoil velocity from photon absorption,  $\ell$  is the distance from the atom-laser interaction point to the first slit, and  $L$  is the distance to the second slit. In this case, the first-order Doppler effect induces a red shift ( $\Delta\nu$ ) to the transition frequency ( $\nu_c$ )

$$\frac{\Delta\nu}{\nu_c} = -\frac{v_R}{c} \frac{L}{\ell + L} \quad (2)$$

When probe 2 is active, only atoms with a reversed velocity can pass the final slit. However, because probe 2 propagates in the opposite direction, the center frequency is red shifted again. This phenomenon illustrates how both probe beams in opposite directions reinforce the same red shift in the detected spectra.

Both the experimental results (Fig. 2F) and the theoretical analysis (detailed in the Supplementary Materials) reveal a systematic frequency shift due to the PS effect, referred to as the PS shift (PSS), which was measured to be  $\Omega_{\text{PSS}} \approx -55$  kHz. This shift, described by Eq. 2, occurs when a very narrow slit 3 is used. PSS is expected to vanish if slit 3 is positioned close to the probing zone or made sufficiently wide to detect all atoms, regardless of their velocity along the  $x$  axis.

To mitigate this, we used a narrow incident atomic beam (32) and a wide slit 3 (about 10 mm) to measure the  $2^3S_1 - 2^3P_0$  transition. With the PSS effect effectively eliminated, we determined the transition frequency of  $^4\text{He}$  to be  $276,764,094,712.45 \pm 0.86$  kHz. By combining these measurements with the fine structure intervals reported in a previous study (34), we calculated the centroid frequency of the  $2^3S - 2^3P$  transition to be  $276,736,495,655.21 \pm 0.87$  kHz. Furthermore, the PSS can be derived and corrected in certain experimental configurations, as outlined in the Supplementary Materials.

## DISCUSSION

Note that although we eliminated PSS in the above measurement, there is no “slit-free” configuration in atomic beam measurements. In this work, we put narrow slits before the probing zone to avoid PSS, with the price of an extended atomic beam length to reduce the Doppler broadening and consequently a reduced atomic beam flux. Moreover, the detector’s limit size and the effective diameter of the SGM may also contribute to a PS effect. Therefore, the PS effect should always be considered in such precision measurements. The PSS should also be presented in the previous measurement by Shiner *et al.* (28, 35) according to their experimental scheme. The effect has also been considered in recent studies of atomic helium by Clausen *et al.* (36).

The precise determination of transition frequencies plays a crucial role in testing the standard model, particularly with respect to accounting for the finite size of the helium nucleus. This finite size results in frequency shifts compared to a point-like nucleus. In isotopic shifts between  $^4\text{He}$  and  $^3\text{He}$  atoms, most mass-independent terms cancel out, allowing for the precise determination of the difference in squared nuclear charge radii between the two isotopes, denoted as  $\delta r^2 [r_h^2 - r_\alpha^2]$ . By combining the  $^4\text{He}$  transition frequency determined in this work with the  $^3\text{He}$  value from Cancio Pastor *et al.* (26), a different  $\delta r^2$  value of  $1.0733 \pm 0.0021$  fm<sup>2</sup> is derived. This result is shown in Fig. 4 as a red circle, compared with results from other groups. Notably, Shiner *et al.* (28, 35), using a similar approach based on the  $2^3S - 2^3P$  transition, derived  $\delta r^2 = 1.061 \pm 0.003$  fm<sup>2</sup>, which notably deviates from our results and may be influenced by the PSS effect. However, because the PSS value can differ between  $^3\text{He}$  and  $^4\text{He}$  isotopes, we cannot estimate a direct PSS correction to Shiner’s result. The  $\delta r^2$  value has also been measured using the forbidden  $2^3S - 2^1S$

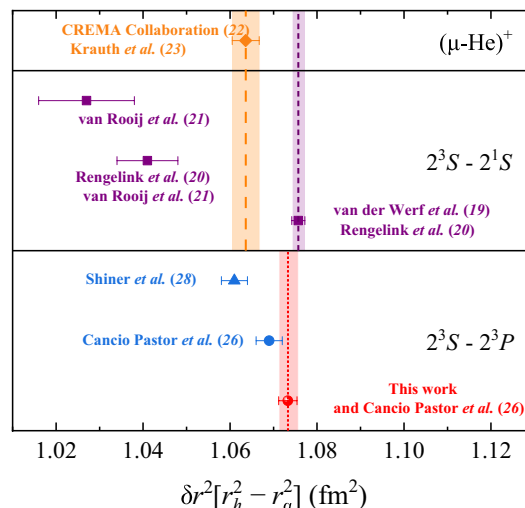


**Fig. 4. The difference between the squared nuclear charge radii of  $^3\text{He}$  and  $^4\text{He}$ .**

The results are derived from isotope shifts in different transitions. The orange diamond represents the result for the muonic helium ion (22, 23). The purple squares represent the results of the  $2^3S - 2^1S$  transition obtained by the Amsterdam group (19–21). The previous result has recently been updated to the new one shown on the right. The bottom panel shows the results obtained by three groups detecting the  $2^3S - 2^3P$  transition. Note that the result of Shiner’s group (28) (triangle) was also affected by the PS effect.

transition in cold atomic clouds (20, 21), with a revised value of  $1.0757 \pm 0.0015$  fm<sup>2</sup> reported recently (19). In addition, the latest measurements from muonic helium ions (22, 23) yield  $\delta r^2 = 1.0636 \pm 0.0031$  fm<sup>2</sup>, showing an approximately  $2.6\sigma$  deviation from the value obtained from electronic helium spectroscopy.

While the cause of this discrepancy remains unclear, it may be necessary to consider the potential PS effect in various experiments (37), such as the helium ion experiment (38), Rydberg-state spectroscopy (39), and hydrogen atom spectroscopy (40). If these deviations between electronic and muonic measurements in both hydrogen and helium are confirmed, it could suggest a nonequivalence of leptons in electromagnetic interactions, pointing to new physics beyond the Standard Model.

## MATERIALS AND METHODS

A schematic configuration of the  $2^3S_1 - 2^3P_0$  spectroscopy experiment of  $^4\text{He}$  is illustrated in Fig. 1. Helium atoms were initially excited to the  $2^3S_1$  state by a radiofrequency discharge. The atoms were then slowed using a Zeeman slower, collimated by a two-dimensional magneto-optical trap, and subsequently deflected by a laser tuned to the  $2^3S_1 - 2^3P_0$  transition. Upon excitation, the atoms were pumped into the  $2^3P_0$  state, and they spontaneously decayed to the  $M = \pm 1$  sublevels of the  $2^3S_1$  state. A probe laser scanned across the  $2^3S_1 - 2^3P_0$  transition, exciting some atoms and causing them to decay to the  $2^3S_1$  ( $M = 0$ ) state. After the probing region, an SGM deflected all atoms in the  $M = \pm 1$  states. Only atoms in the  $M = 0$  state could pass through the SGM region and reach the MCP detector. More details about the experimental setup can be found in (33, 41). The data analysis process is described in the first section of the Supplementary Materials.

Theoretical investigation in this work used both the PS model and the Monte Carlo wave function (MCWF) method. The PS model simplifies various experimental complexities, such as the distribution of

the atomic beam, spontaneous radiation, and momentum conversion, enabling the simulation of spectroscopy results under diverse experimental conditions. The MCWF method provides a more detailed simulation, similar to density matrix calculations, by accounting for the spontaneous radiation and momentum conversion. The MCWF approach has been applied to model light force-induced shifts (42). While the PS model offers a generalized framework, it may deviate from experimental results under certain conditions. The MCWF method aligns more closely with experimental conditions but comes with increased computational complexity. Comprehensive details of both approaches are provided in the Supplementary Materials.

## Supplementary Materials

This PDF file includes:

Supplementary Text

Figs. S1 to S4

Tables S1 to S3

References

## REFERENCES AND NOTES

1. Y. Aharonov, D. Z. Albert, L. Vaidman, How the result of a measurement of a component of the spin of a spin-1/2 particle can turn out to be 100. *Phys. Rev. Lett.* **60**, 1351–1354 (1988).
2. J. Dressel, M. Malik, F. M. Miatto, A. N. Jordan, R. W. Boyd, Colloquium: Understanding quantum weak values: Basics and applications. *Rev. Mod. Phys.* **86**, 307–316 (2014).
3. Y. Aharonov, S. Popescu, J. Tollaksen, A time-symmetric formulation of quantum mechanics. *Phys. Today* **63**, 27–32 (2010).
4. T. Denkmayr, H. Geppert, S. Sponar, H. Lemmel, A. Matzkin, J. Tollaksen, Y. Hasegawa, Observation of a quantum Cheshire Cat in a matter-wave interferometer experiment. *Nat. Commun.* **5**, 4492 (2014).
5. L. Vaidman, Weak value controversy. *Phil. Transact. Roy. Soc. A* **375**, 20160395 (2017).
6. O. Hosten, P. Kwiat, Observation of the spin hall effect of light via weak measurements. *Science* **319**, 787–790 (2008).
7. S. Kocsis, B. Braverman, S. Ravets, M. J. Stevens, R. P. Mirin, L. K. Shalm, A. M. Steinberg, Observing the average trajectories of single photons in a two-slit interferometer. *Science* **332**, 1170–1173 (2011).
8. M. E. Goggin, M. P. Almeida, M. Barbieri, B. P. Lanyon, J. L. O'Brien, A. G. White, G. J. Pryde, Violation of the Leggett-Garg inequality with weak measurements of photons. *Proc. Natl. Acad. Sci. U.S.A.* **108**, 1256–1261 (2011).
9. J. S. Lundeen, B. Sutherland, A. Patel, C. Stewart, C. Bamber, Direct measurement of the quantum wavefunction. *Nature* **474**, 188–191 (2011).
10. A. Feizpour, X. Xing, A. M. Steinberg, Amplifying single-photon nonlinearity using weak measurements. *Phys. Rev. Lett.* **107**, 133603 (2011).
11. A. N. Jordan, J. Martínez-Rincón, J. C. Howell, Technical advantages for weak-value amplification: When less is more. *Phys. Rev. X* **4**, 011031 (2014).
12. M. Hallaji, A. Feizpour, G. Dmochowski, J. Sinclair, A. M. Steinberg, Weak-value amplification of the nonlinear effect of a single photon. *Nat. Phys.* **13**, 540–544 (2017).
13. Z.-H. Liu, W. W. Pan, X. Y. Xu, M. Yang, J. Zhou, Z. Y. Luo, K. Sun, J. L. Chen, J. S. Xu, C. F. Li, G. C. Guo, Experimental exchange of grins between quantum Cheshire cats. *Nat. Commun.* **11**, 3006 (2020).
14. W. Markowitz, R. G. Hall, L. Essen, J. V. L. Parry, Frequency of cesium in terms of ephemeris time. *Phys. Rev. Lett.* **1**, 105–107 (1958).
15. M. S. Safronova, D. Budker, D. DeMille, D. F. J. Kimball, A. Derevianko, C. W. Clark, Search for new physics with atoms and molecules. *Rev. Mod. Phys.* **90**, 025008 (2018).
16. F. Ficek, D. F. J. Kimball, M. G. Kozlov, N. Leefer, S. Pustelny, D. Budker, Constraints on exotic spin-dependent interactions between electrons from helium fine-structure spectroscopy. *Phys. Rev. A* **95**, 032505 (2017).
17. G. S. Adkins, D. B. Cassidy, J. Perez-Rios, Precision spectroscopy of positronium: Testing bound-state QED theory and the search for physics beyond the Standard Model. *Phys. Rep.* **975**, 1–61 (2022).
18. N. L. Figueroa, J. C. Berengut, V. A. Dzuba, V. V. Flambaum, D. Budker, D. Antypas, Precision determination of isotope shifts in ytterbium and implications for new physics. *Phys. Rev. Lett.* **128**, 073001 (2022).
19. Y. van der Werf, K. Steinebach, R. Jannin, H. L. Bethlem, K. S. E. Eikema, The alpha and helion particle charge radius difference from spectroscopy of quantum-degenerate helium. arXiv:2306.02333 (2023).
20. R. J. Rengelink, Y. van der Werf, R. P. M. J. W. Notermans, R. Jannin, K. S. E. Eikema, M. D. Hoogerland, W. Vassen, Precision spectroscopy of helium in a magic wavelength optical dipole trap. *Nat. Phys.* **14**, 1132–1137 (2018).
21. R. van Rooij, J. S. Borbely, J. Simonet, M. D. Hoogerland, K. S. Eikema, R. A. Rozendaal, W. Vassen, Frequency metrology in quantum degenerate helium: Direct measurement of the  $2^3S_1 - 2^1S_0$  transition. *Science* **333**, 196–198 (2011).
22. CREMA Collaboration, The helion charge radius from laser spectroscopy of muonic helium-3 ions. arXiv:2305.11679 [physics.atom-ph] (2023).
23. J. J. Krauth, K. Schuhmann, M. A. Ahmed, F. D. Amaro, P. Amaro, F. Biraben, T. L. Chen, D. S. Covita, A. J. Dax, M. Diepold, L. M. P. Fernandes, B. Franke, S. Galtier, A. L. Gouvea, J. Götzfried, T. Graf, T. W. Hänsch, J. Hartmann, M. Hildebrandt, P. Indelicato, L. Julien, K. Kirch, A. Knecht, Y. W. Liu, J. Machado, C. M. B. Monteiro, F. Mulhauser, B. Naar, T. Nebel, F. Nez, J. M. F. dos Santos, J. P. Santos, C. I. Szabo, D. Taqqu, J. F. C. A. Veloso, J. Vogelsang, A. Voss, B. Weichelt, R. Pohl, A. Antognini, F. Kottmann, Measuring the alpha-particle charge radius with muonic helium-4 ions. *Nature* **589**, 527–531 (2021).
24. A. Matveev, C. G. Parthey, K. Predehl, J. Alnis, A. Beyer, R. Holzwarth, T. Udem, T. Wilken, N. Kolachevsky, M. Abgrall, D. Rovera, C. Salomon, P. Laurent, G. Grosche, O. Terra, T. Legero, H. Schnatz, S. Weyers, B. Altschul, T. W. Hänsch, Precision measurement of the hydrogen 1S-2S frequency via a 920-km fiber link. *Phys. Rev. Lett.* **110**, 230801 (2013).
25. A. Antognini, F. Nez, K. Schuhmann, F. D. Amaro, F. Biraben, J. M. R. Cardoso, D. S. Covita, A. Dax, S. Dhawan, M. Diepold, L. M. P. Fernandes, A. Giesen, A. L. Gouvea, T. Graf, T. W. Hänsch, P. Indelicato, L. Julien, C. Y. Kao, P. Knowles, F. Kottmann, E. O. le Bigot, Y. W. Liu, J. A. M. Lopes, L. Ludhova, C. M. B. Monteiro, F. Mulhauser, T. Nebel, P. Rabinowitz, J. M. F. dos Santos, L. A. Schaller, C. Schwob, D. Taqqu, J. F. C. A. Veloso, J. Vogelsang, R. Pohl, Proton structure from the measurement of 2S-2P transition frequencies of muonic hydrogen. *Science* **339**, 417–420 (2013).
26. P. Cancio Pastor, L. Consolino, G. Giusfredi, P. De Natale, M. Inguscio, V. A. Yerokhin, K. Pachucki, Frequency metrology of helium around 1083 nm and determination of the nuclear charge radius. *Phys. Rev. Lett.* **108**, 143001 (2012).
27. K. Pachucki, V. Lensky, F. Hagelstein, S. S. Li Muli, S. Bacca, R. Pohl, Comprehensive theory of the Lamb shift in light muonic atoms. *Rev. Mod. Phys.* **96**, 015001 (2024).
28. D. Shiner, R. Dixon, V. V. Vedantham, Three-nucleon charge radius: A precise laser determination using  $^3\text{He}$ . *Phys. Rev. Lett.* **74**, 3553–3556 (1995).
29. Y.-J. Huang, Y.-C. Guan, J.-L. Peng, J.-T. Shi, L.-B. Wang, Precision laser spectroscopy of the  $2^1S_0-3^1D_2$  two-photon transition in  $^3\text{He}$ . *Phys. Rev. A* **101**, 062507 (2020).
30. I. Sick, Zernike moments of  $^3\text{He}$  and  $^4\text{He}$ . *Phys. Rev. C* **90**, 064002 (2014).
31. N. F. Ramsey, A new molecular beam resonance method. *Phys. Rev.* **76**, 996–996 (1949).
32. J.-L. Wen, J. D. Tang, J. F. Dong, X. J. du, S. M. Hu, Y. R. Sun, Doppler-free spectroscopy of an atomic beam probed in traveling-wave fields. *Phys. Rev. A* **107**, 042811 (2023).
33. J. J. Chen, Y. R. Sun, J. L. Wen, S. M. Hu, Speed-adjustable atomic beam of metastable helium for precision measurement. *Phys. Rev. A* **101**, 053824 (2020).
34. X. Zheng, Y. R. Sun, J.-J. Chen, W. Jiang, K. Pachucki, S.-M. Hu, Laser spectroscopy of the fine-structure splitting in the  $2^3P_J$  levels of  $^4\text{He}$ . *Phys. Rev. Lett.* **118**, 063001 (2017).
35. D. Shiner, R. Dixon, P. Zhao, Precise measurement of the Lamb shift and fine structure of the 2S-2P transition in triplet helium. *Phys. Rev. Lett.* **72**, 1802–1805 (1994).
36. G. Clausen, S. Scheidegger, J. A. Agner, H. Schmutz, F. Merkt, Imaging-assisted single-photon Doppler-free laser spectroscopy and the ionization energy of metastable triplet helium. *Phys. Rev. Lett.* **131**, 103001 (2023).
37. E. Tiesinga, P. J. Mohr, D. B. Newell, B. N. Taylor, CODATA recommended values of the fundamental physical constants: 2018. *Rev. Mod. Phys.* **93**, 025010 (2021).
38. A. van Wijngaarden, F. Holuj, G. W. F. Drake, Lamb shift in He<sup>+</sup>: Resolution of a discrepancy between theory and experiment. *Phys. Rev. A* **63**, 012505 (2000).
39. E. A. Hessels, P. W. Arcuni, F. J. Deck, S. R. Lundeen, Microwave spectroscopy of high-*L*, *n*=10 Rydberg states of helium. *Phys. Rev. A* **46**, 2622–2641 (1992).
40. D. J. Berkeland, E. A. Hinds, M. G. Boshier, Precise optical measurement of lamb shifts in atomic hydrogen. *Phys. Rev. Lett.* **75**, 2470–2473 (1995).
41. X. Zheng, Y. R. Sun, J.-J. Chen, W. Jiang, K. Pachucki, S.-M. Hu, Measurement of the frequency of the  $2^3S_1 - 2^3P$  transition of  $^4\text{He}$ . *Phys. Rev. Lett.* **119**, 263002 (2017).
42. X. Zheng, Y. R. Sun, J. J. Chen, J. L. Wen, S. M. Hu, Light-force-induced shift in laser spectroscopy of atomic helium. *Phys. Rev. A* **99**, 032506 (2019).
43. A. Marsman, M. Horbatsch, E. A. Hessels, Shifts due to distant neighboring resonances for laser measurements of  $2^3S_1$ -to- $2^3P_J$  transitions of helium. *Phys. Rev. A* **86**, 040501 (2012).
44. P. Cancio Pastor, G. Giusfredi, P. De Natale, G. Hagel, C. de Mauro, M. Inguscio, Absolute frequency measurements of the  $2^3S_1 \rightarrow 2^3P_{0,1,2}$  atomic helium transitions around 1083 nm. *Phys. Rev. Lett.* **92**, 230011–230014 (2004).
45. P. Cancio Pastor, G. Giusfredi, P. De Natale, G. Hagel, C. de Mauro, M. Inguscio, Erratum: Absolute frequency measurements of the  $2^3S_1 \rightarrow 2^3P_{0,1,2}$  atomic helium transitions around 1083nm [Phys. Rev. Lett.92, 023001 (2004)]. *Phys. Rev. Lett.* **97**, 139903 (2006).
46. K. Pachucki, V. Patkóš, V. A. Yerokhin, Testing fundamental interactions on the helium atom. *Phys. Rev. A* **95**, 062510 (2017).
47. V. Patkóš, V. A. Yerokhin, K. Pachucki, Complete  $a^7m$  Lamb shift of helium triplet states. *Phys. Rev. A* **103**, 042809 (2021).

**Acknowledgments:** The numerical calculations in this paper have been carried out on the supercomputing system in the Supercomputing Center of the University of Science and Technology of China. **Funding:** This work was jointly supported by the Innovation Program for Quantum Science and Technology (grant no. 2021ZD0303102), the National Natural Science Foundation of China (grants nos. 12393822, 12374465, and 22241301), and the Strategic Priority Research Program of the Chinese Academy of Sciences (grant nos. XDB21010400 and XDC07010000). Y.-N.L. was also supported by the Postdoctoral Fellowship Program of CPSF (grant no. GZC20232563). C.-L.Z. also acknowledges support from the Fundamental Research Funds for the Central Universities and the USTC Center for Micro and Nanoscale Research and Fabrication. **Author contributions:** J.-L.W. conducted the experiment and data analysis. J.-D.T. conducted the MCWF simulation. Y.-N.L. performed the postselection theory calculation. Y.R.S.

supervised the experiment and data analysis. C.-L.Z. supervised the theoretical analysis. J.-F.D. contributed to the experiment and data analysis. S.-M.H. supervised the experiment and proposed the phenomenological model. All authors contributed to writing the manuscript.

**Competing interests:** The authors declare that they have no competing interests. **Data and materials availability:** All data needed to evaluate the conclusions in the paper are present in the paper and/or the Supplementary Materials.

Submitted 3 December 2024

Accepted 28 January 2025

Published 28 February 2025

10.1126/sciadv.adu9796